Supplemental Figures

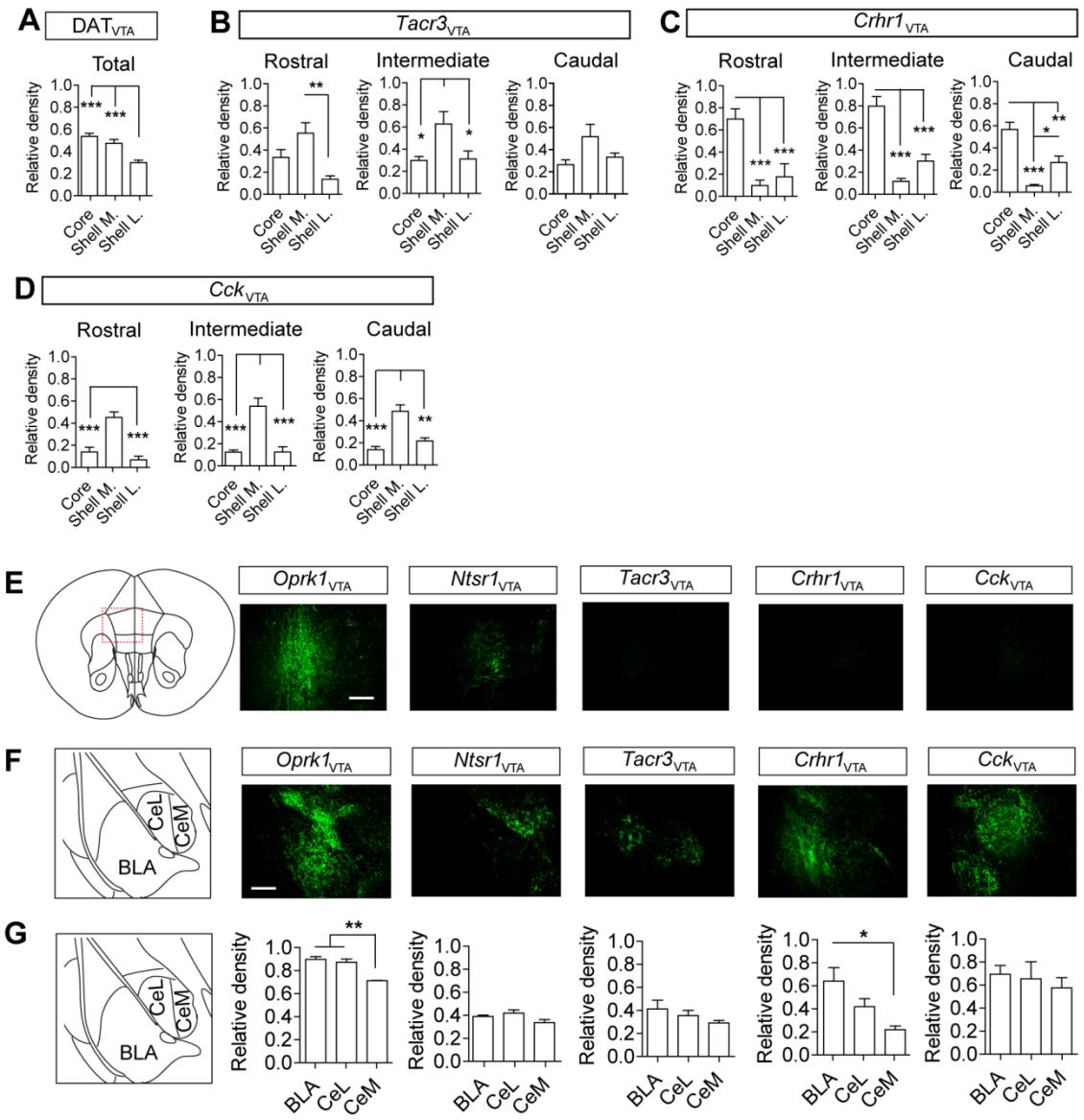

Figure S1. Anatomical characterization of VTA subpopulation innervation of VTA-receptive brain regions related to Figure 2. (A) Innervation density of the NAc core and shell in DAT-cre mice injected with AAV1-FLEX- synaptophysin-GFP (one-way ANOVA, $F_{(2,33)}$=18.5, P<0.0001, ***P<0.001, n=12). (B-D) Innervation density of the NAc

core and shell along the rostral, intermediate and caudal extent of the NAc in *Tacr3-Cre* injected mice (n=4, one-way ANOVA, rostral: $F_{(2,9)}$= 8.93, P<0.01, Bonferroni multiple comparisons **P<0.01; intermediate: $F_{(2,9)}$= 5.47, P<0.05, Bonferroni multiple comparisons *P<0.05; caudal: not significant), *Crhr1*-Cre injected mice (n=5, one-way ANOVA, rostral: $F_{(2,12)}$= 64.93, P<0.0001, Bonferroni multiple comparisons ***P<0.001; intermediate: $F_{(2,12)}$= 30.37, P<0.0001, Bonferroni multiple comparisons ***P<0.001; caudal: $F_{(2,12)}$= 24.8, P<0.001, Bonferroni multiple comparisons ***P<0.001, **P<0.01, P<0.05), *Cck*-Cre injected mice (n=5, rostral: $F_{(2,12)}$= 23.57, P<0.0001, Bonferroni multiple comparisons ***P<0.001; intermediate: $F_{(2,12)}$= 21.12, P<0.0001, Bonferroni multiple comparisons ***P<0.001; caudal: $F_{(2,12)}$= 19.64, P<0.001, Bonferroni multiple comparisons ***P<0.001, **P<0.01). (E) Schematic illustrating location of dopamine input to the prefrontal cortex (left). Only $Oprk_{VTA}$ neurons showed innervation of the cortex as visualized with synaptophysin-GFP (right). Scale = 250μm. (F) Schematic (left) illustrating location of dopamine input to the amygdala subdivisions (BLA: basolateral amygdala, CeL: central lateral nucleus, CeM: central medial nucleus). Example images (right) illustrating terminal synaptophysin-GFP expression in the d amygdala (Scale = 250μm). (G) Quantification of synaptophysin-GFP in subdivisions of the amygdala in Cre-driver lines (n=3 mice, 9 sections/animal; one-way ANOVA *Oprk1*: $F_{(2,8)}$=3.74, P<0.05; *Crhr1:* $F_{(2,8)}$=7.84, P<0.01 Tukey's multiple comparisons *P<.05, **P<0.01).

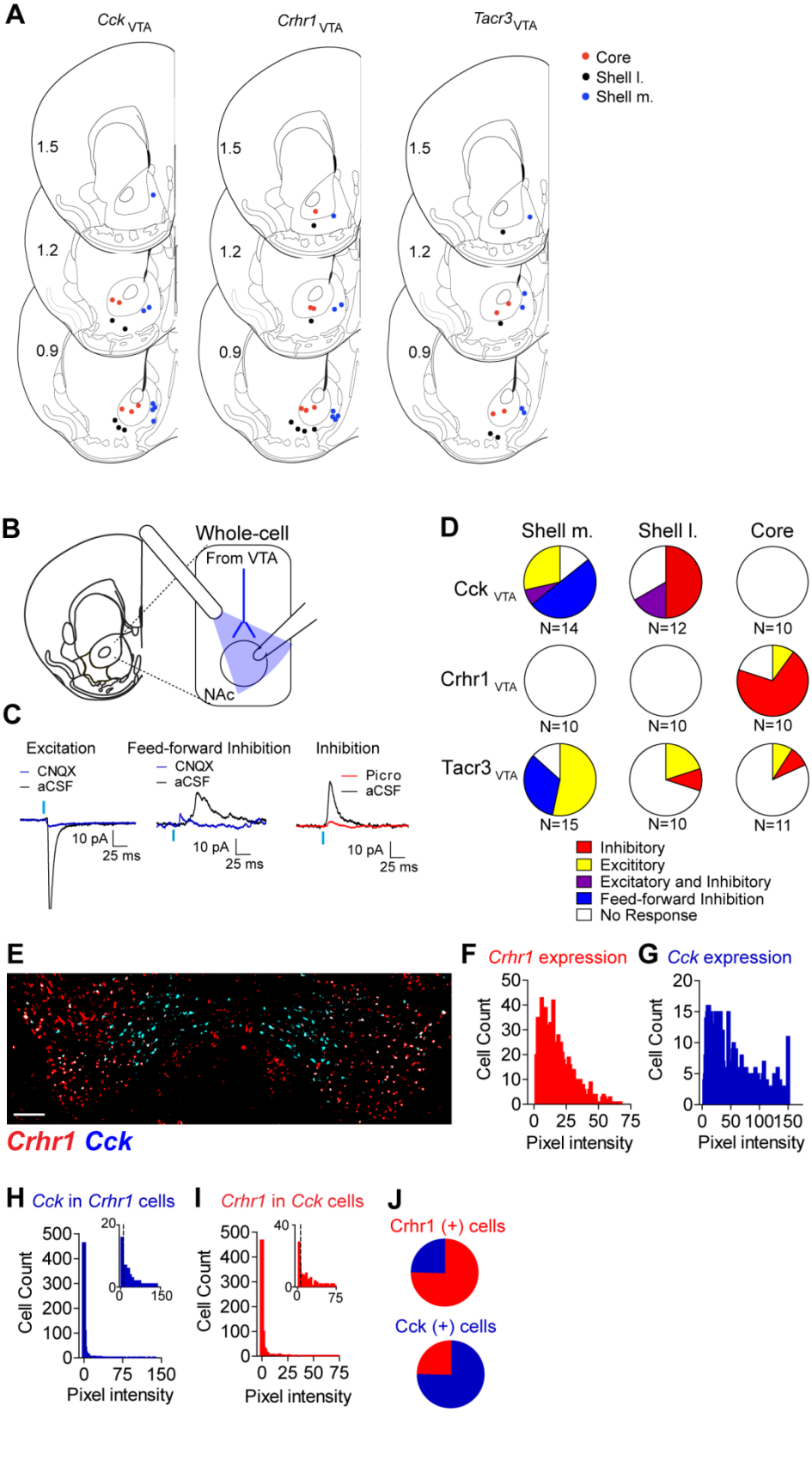
A
Cck VTA
Crhr1 VTA
Tacr3 VTA
Core
Shell l.
Shell m.
1.5
1.2
0.9
B
Whole-cell
From VTA
NAc
C
Excitation
Feed-forward Inhibition
Inhibition
CNQX
aCSF
Picro
10 pA
25 ms
D
Shell m.
Shell l.
Core
Cck VTA
Crhr1 VTA
Tacr3 VTA
N=14
N=12
N=10
N=10
N=10
N=10
N=15
N=10
N=11
Inhibitory
Excitory
Excitatory and Inhibitory
Feed-forward Inhibition
No Response
E
Crhr1 Cck
F Crhr1 expression
G Cck expression
Cell Count
Pixel intensity
H Cck in Crhr1 cells
I Crhr1 in Cck cells
J
Crhr1 (+) cells
Cck (+) cells

Figure S2. Anatomical location of FSCV recordings in the NAc and synaptic connectivity of VTA projection neurons in the NAc and expression of *Crhr1* and *Cck* in the VTA related to Figure 2. Anatomical locations in designated regions (red, Core; blue, Shell M.; and black, Shell L.) for *Cck*-Cre, *Crhr*-Cre, and *Tacr3*-Cre mice. (B) Schematic for recording light-evoked post-synaptic responses in NAc subregions. (C) Example traces for *Tacr3* LiEPSC (left), *Cck* feed-forward inhibition (middle), and *Crhr1* LiIPSC (right). Excitatory responses were blocked by the glutamate receptor antagonist CNQX and inhibitory responses were blocked by the GABA antagonist picrotoxin (Picro) (D) Postsynaptic response proportions following stimulation of Cck_{VTA}, $Crhr1_{VTA}$ and $Tacr3_{VTA}$ terminals. (E) Example image of a rostral VTA coronal section with *Crhr1* and *Cck* mRNA signals, 10x magnification (Scale bar: 100μm). (E-F) Distribution of *Crhr1* (F) and *Cck* (G) expression levels per cell plotted as mean pixel intensity. Regions of interest (ROIs, 8μm diameter) with one visible puncta of signal were measured to establish the minimal detectable signals for each marker (*Crhr1* range: 2-6 mean pixel intensity; *Cck* range: 4-11 mean pixel intensity). Cells with a mean pixel intensity for *Crhr1* >2 were counted as positive and cells a mean pixel intensity for *Cck* >4 were counted as positive. Based on these thresholds 15.4% of *Crhr1*-positive neurons are low *Crhr1* expressing cells (between 2 and 6 mean pixel intensity), and 9.6% of *Cck*-positive neurons are low *Cck* expressing cells (between 4 and 11 mean pixel intensity). (H) Distribution of *Cck* expression in all *Crhr1*-positive neurons. Inset: Distribution of *Cck* expression in cells designated *Cck*-postitive in *Crhr1*-expressing neurons. Dashed line designates threshold for “low” *Cck* expressing cells (mean pixel intensity <11). (I) Distribution of *Crhr1* expression in all *Cck*-positive

neurons. Inset: Distribution of *Crhr1* expression in cells designated *Crhr1*-postitive in *Cck*-expressing neurons. Dashed line designates threshold for “low” *Crhr1* expressing cells (mean pixel intensity <6). (J) Proportion of cells expressing *Cck* (blue, >4 mean pixel intensity) in *Crhr1*-positive neurons (red, top) and the proportion of cells expressing *Crhr1* (red, >2 mean pixel intensity) *in Cck*-positive neurons (blue, bottom).

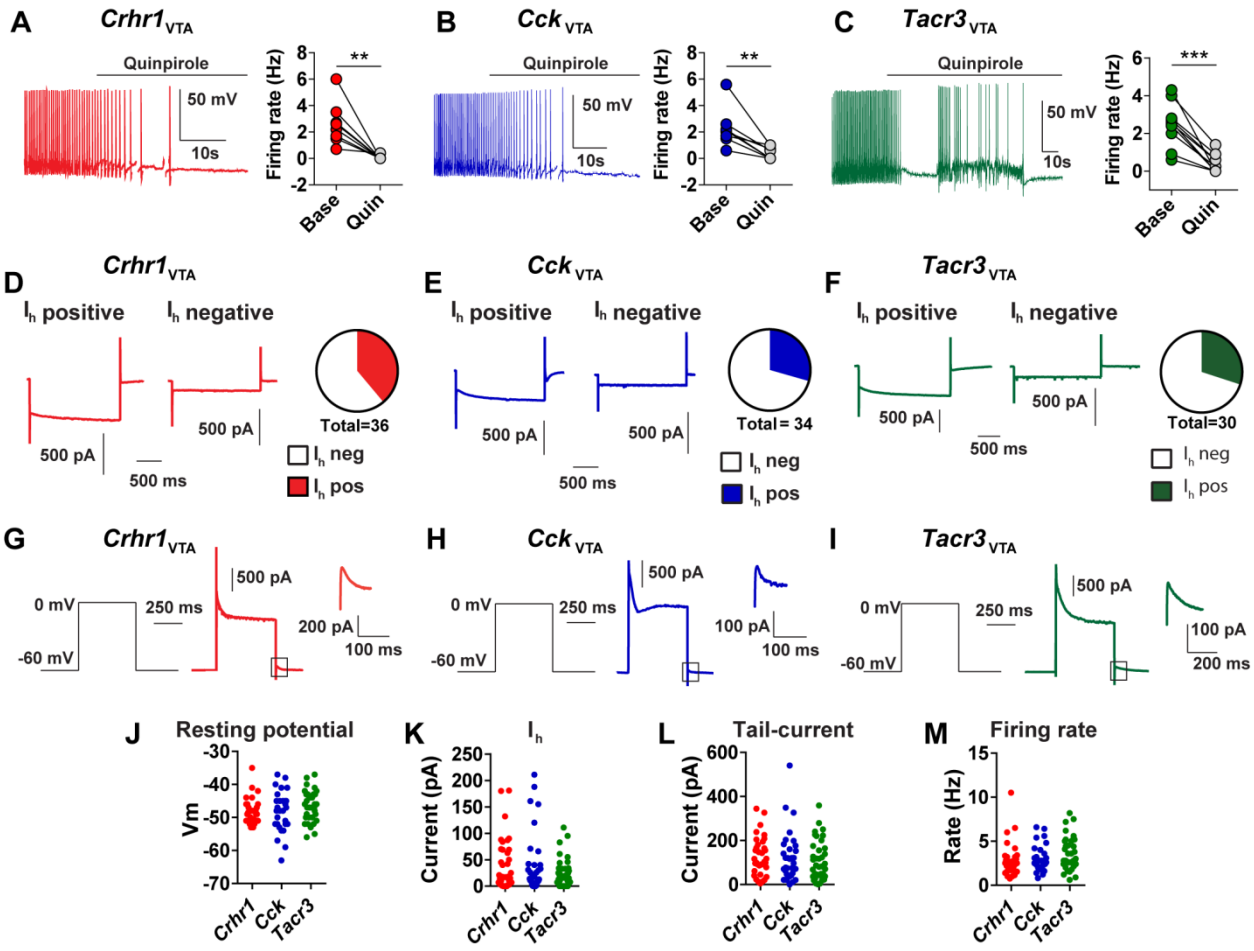

Figure S3. Characterization of *Crhr1*$_{VTA}$, *Cck*$_{VTA}$, and *Tacr3*$_{VTA}$ intrinsic physiological properties related to Figure 2. (A-C) Left: Example traces illustrating sensitivity to the D2 agonist Quinpirole (1 mM). Right: Firing rate before and after Quinpirole application. (*Crhr1* (A): n=3 mice, 8 cells; *Cck* (B): n=3 mice, 8 cells; *Tacr3* (C): n=2 mice, 10 cells; student's paired t-test, two-tailed, **P<0.01, ***P<.001). (D-F) Example traces for hyperpolarization-activated (I_h) current positive (left trace) and negative (right trace) for *Crhr1*$_{VTA}$ (D), *Cck*$_{VTA}$ (E), or *Tacr3*$_{VTA}$ (F) neurons. Pie chart (right) quantifies proportion of I_h positive or negative neurons (*Crhr1*: n=6 mice, 36 cells; *Cck*: n=6 mice, 34 cells, *Tacr3*: n=5 mice, 30 cells). (G-I) Tail current voltage-step protocol (left) and example current trace (right) for *Crhr1*$_{VTA}$ (d), *Cck*$_{VTA}$ (e), or *Tacr3*$_{VTA}$

(c) neurons. Inset: magnified current trace highlighted by black box. (J) Resting membrane potential (*Crhr1*: n=6 mice, 32 cells; C*ck*: n=6 mice, 30 cells; *Tacr3*: n=5 mice, 37 cells). (K) I_h current quantified from D-F. (L) Tail current quantified from G-I (*Crhr1*: n=6 mice, 35 cells; *Cck*: n=6 mice, 34 cells; *Tacr3*: n=5 mice, 38 cells). (M) Firing rate of neurons recorded in D-F.

Figure S4

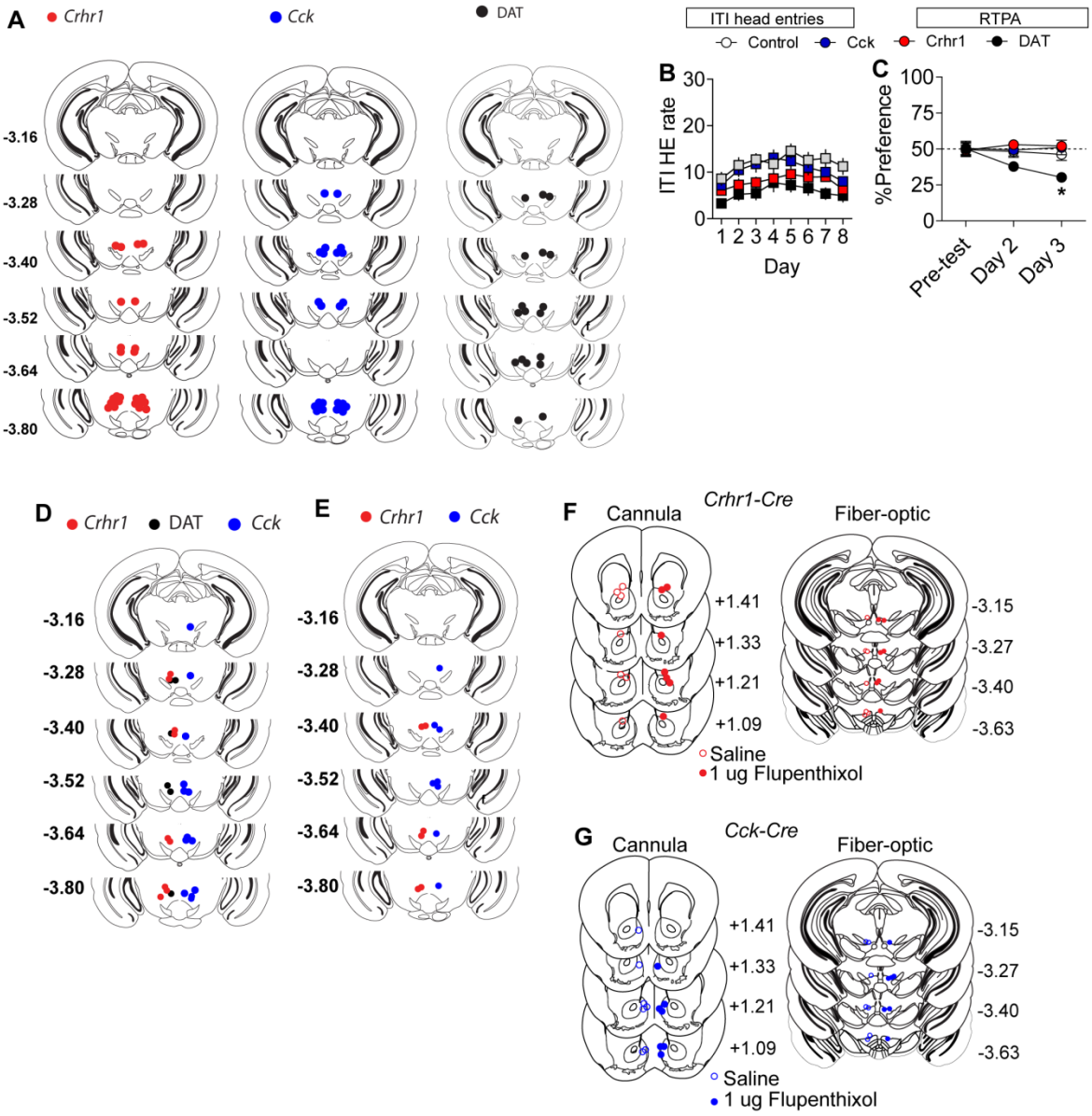

Figure S4. Optic fiber placements related to behavioral data presented in Figures 3, 4, and 5. (A) Bilateral optic fiber placements in *Crhr1*-Cre (left) and *Cck*-Cre (right) mice. (B) Head rate (pre min) into the food hopper during the ITI period of Pavlovian conditioning of mice presented in Figure 3. (C) RTPA with optical inhibition (*Crhr1*, *Cck* and control: n=12 mice/group; DAT: n=9, two-way ANOVA $F_{(6,80)}$=2.62, P=0.0225; Bonferroni multiple comparisons, *P<0.05 relative to all other groups. (D) Optic fiber

placement in mice used in experiments associated with Figure 4C-I. (E) Optic fiber placement in mice used in experiments associated with Figure 4K-M. (F) Optical fiber placements for *Crhr1*-Cre mice in the VTA and infusion cannula placement in the NAc Core. Open circles represent placements for saline injected controls and closed circles represent placements for Flpx injected mice. (G) Optical fiber placements for *Cck*-Cre mice in the VTA and infusion cannula placement in the NAc Core. Open circles represent placements for saline injected controls and closed circles represent placements for Flpx injected mice.

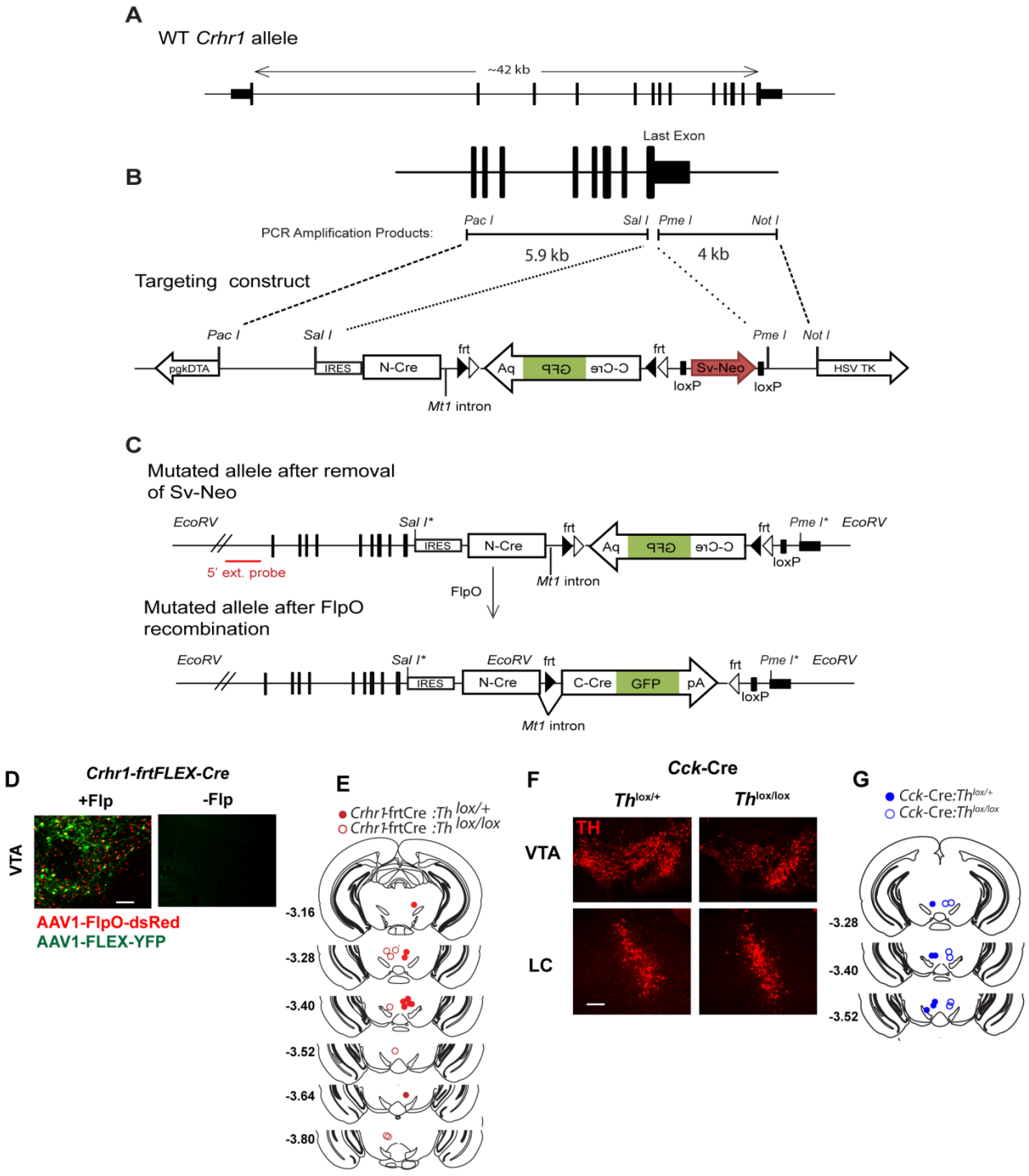

Figure S5. Generation of *Crhr1*-frtCre mice, *Th* expression, and optic fiber placement verification related to Figure 5. (A) Schematic illustration of WT *Crhr1* allele. (B) IRES-frtFLEX-Cre-GFP was inserted into the 3' untranslated region of *Crhr1* to generate a Flp-inducible Cre recombinase as described in extended data figure 11.

(C) Following removal of the loxp-flanked Neo cassette by crossing to *Meox*-Cre mice, offspring were crossed to Th^{lox} mice to allow for cell and region specific gene inactivation. (D) Injection of AAV1-FlpO-dsRed turns on Cre-recombinase allowing for conditional gene inactivation and expression (Scale = 50μm). (E) Optic fiber placements for mice used in figure 5D. (F) Optic fiber locations for mice used in Figure 5F and G. (G) Biallelic *Th* excision in *Cck*-Cre mice results in reduced TH expression in the VTA (top), but no loss in the locus coeruleus (LC: bottom). Scale = 100μm.

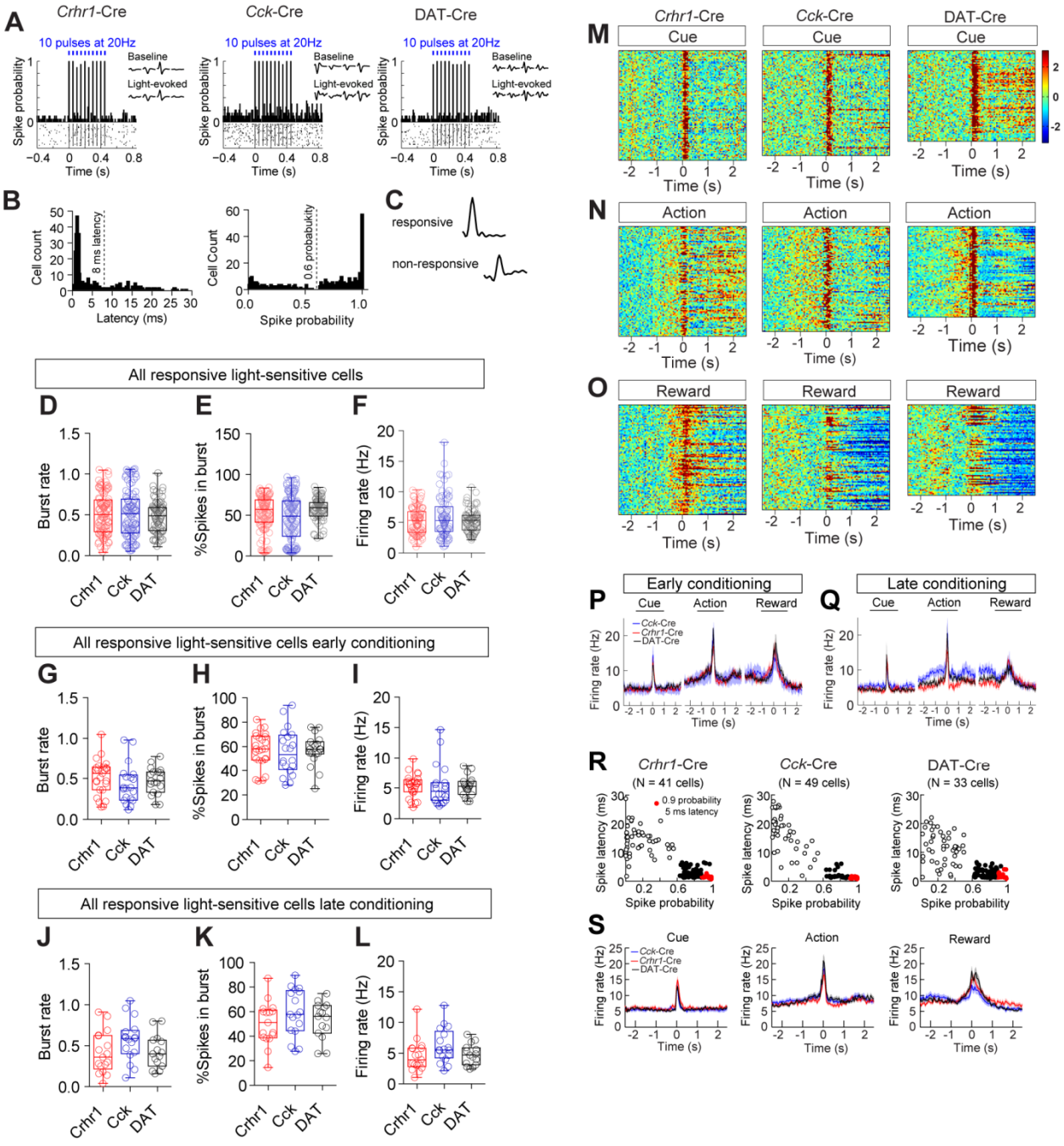

Figure S6. *In vivo* recording of baseline activity in *Crhr1*$_{VTA}$, *Cck*$_{VTA}$, and DAT$_{VTA}$ neurons related to Figure 6. (A) Examples of photo-tagged neurons in the VTA from *Crhr1*-, *Cck*-, and DAT-Cre mouse lines illustrating spike probability in response to 20 Hz optical stimulation for 0.5 s during 10 stimulus sweeps. Inset shows corresponding action potential waveforms from tetrode recordings during baseline and light stimulation

periods. (B) Distribution of cells counts for spike latency (left) and spike probability (right) of recorded neurons. We observed a sharp peak of short-latency responsive cells and the tail of this peak distribution showed a natural deflection point at 8 ms which was set as a criterion for light-responsive units. We observed a flat distribution of cells counts for spike probability that displayed a natural inflection point at 0.6 which was set another criterion for light-responsive units. Cells meeting both criterion, spike latency <0.8 ms and a spike probility >0.6, were considered light responsive. (C) Average waveform of light-responsive and non-responsive cells. (D) Burst rate, or burst epochs per second defined based on defined criterion (Grace and Bunney, 1984) is not different between groups (*Crhr1*-Cre, n=4 mice, N=100 cells; *Cck*-Cre, n=3 mice, N=117 cells; DAT-Cre, n=3 mice, N=85 cells). (E) Percentage of spikes fired in burst. (F) Average firing rate during baseline period. (G-I) Baseline electrophysiological properties as defined in D-F in all light-sensitive neurons during early conditioning (first two days of recording, G-I, *Crhr1*-Cre, n=4 mice, N=28 cells; *Cck*-Cre, n=3 mice, N=24 cells; DAT-Cre, n=3 mice, N=20 cells) and late conditioning (last two days, J-L, *Crhr1*-Cre, n=4 mice, N=18 cells; *Cck*-Cre, n=3 mice, N=24 cells; DAT-Cre, n=3 mice, N=16 cells). (M-O) Heat maps demonstrating firing rate over the course of training to cue (M), action (N), and reward (O). Each row represents the activity of one responsive (greater than 2.5 standard deviations increase from baseline firing rate) cell averaged over the 1-hour recording/conditioning session (*Crhr1*-Cre, n=4 mice, N=100 cells; *Cck*-Cre, n=3 mice, N=117 cells; DAT-Cre, n=3 mice, N=85 cells). (P-Q) Average response of cells designated as responsive (Z-score > 2.5) to each individual event during early conditioning (P) and late conditioning (Q) was not different between groups (Early: Cue:

Cck-Cre n=13, *Crhr1*-Cre n=17, DAT-Cre n=12; Action: *Cck*-Cre n=14, *Crhr1*-Cre n=17, DAT-Cre n=12; Reward: *Cck*-Cre n=11, *Crhr1*-Cre n=20, DAT-Cre n=14; Late: Cue: *Cck*-Cre n=12, *Crhr1*-Cre n=10, DAT-Cre n=15; Action: *Cck*-Cre n=16, *Crhr1*-Cre n=11, DAT-Cre n=13; Reward: *Cck*-Cre n=4, *Crhr1*-Cre n=10, DAT-Cre n=4). (R) Spike latecy versus spike probability highlighting (red) cells selected under stringent light-responsive criterion (spike probability >0.9 and spike latency <5 ms). (S) Phasic responses of cells during the designated events across conditioning identified as light responsive using stringent criterion are similar to those observed under our light-sensitive designation of spike latency <8 ms and spike probability >0.6 presented in Figure 6D.

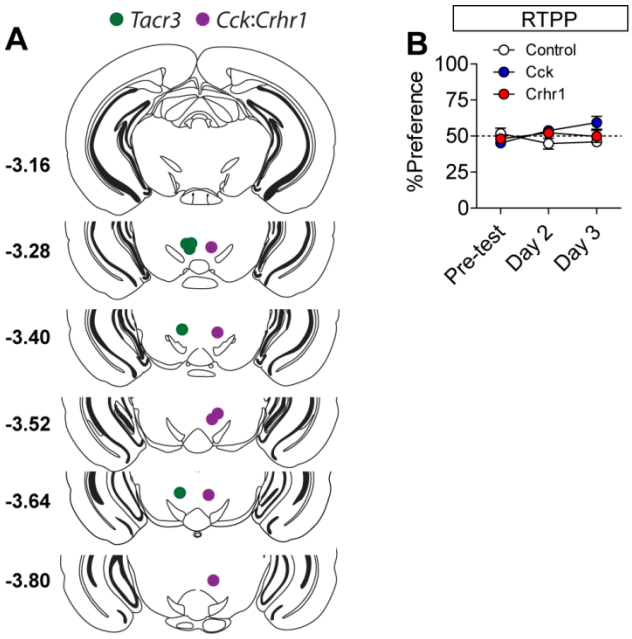

Figure S7. Optic fiber placements and cell counts related to Figure 7. (A) Optic fiber placements in *Tacr3* and *Crhr1*::*Cck* groups used in Figure 7. (B) RTPP of *Crhr1*-Cre and *Cck*-Cre mice expressing ChR2-mCherry in the VTA of mCherry (controls). There is no significant difference between the groups (two-way repeated measures ANOVA, $F_{(2,38)}$=1.21, P=0.308).